American Mineralogist, Volume 75, pages 1349–1361, 1990

Amphibolite-facies-to-granulite-facies reactions in experimentally deformed, unpowdered amphibolite

BRADLEY R. HACKER*
Department of Earth and Space Sciences, University of California, Los Angeles, California 90024-1567, U.S.A.

ABSTRACT

Reactions in mafic amphibolite marking the transition from amphibolite to granulite facies were investigated by hydrostatically heating and deforming solid cylinders of An_{30} plagioclase + tschermakitic hornblende + minor quartz for up to 795 h at temperatures of 700–1000 °C and mean stresses of 0.7–2.1 GPa. Melting of quartz + plagioclase + amphibole began at 775 °C in the presence of H_2O and at 900 °C under H_2O-undersaturated conditions. The amphibole crystals underwent Mg-Tschermak substitution and the plagioclase crystals became more anorthitic. At 875–1000 °C, the rock became a partially melted granulite with hornblende, anorthitic plagioclase, augite, and hypersthene. The augite and hypersthene nucleated on amphibole crystals in liquid films adjacent to quartz crystals. During subsequent growth (and decreasing surface/volume ratio) the pyroxene crystals abandoned their coherent interfaces with their host amphibole crystal for energetically more favorable and more mobile incoherent interfaces and grew outward into the enveloping liquid that was produced by the breakdown of plagioclase + amphibole + quartz. There is a measurable effect of stress and deformation on these reactions. Some phases grown in deformed samples have slightly, but systematically, different compositions from phases grown in hydrostatically heated samples. Unfortunately, the system is too complex to assess the implications for natural metamorphism. Comparison with equilibrium petrology experiments indicates that the reactions were incomplete and the compositions and proportions of the phases produced during the experiments are metastable. This suggests that amphibolite-facies-to-granulite-facies equilibrium textures and phase compositions cannot be experimentally investigated in unpowdered mafic rock because reaction rates are too slow, unless experiments can be conducted for longer than one month.

INTRODUCTION

This paper reports the results of deformation and hydrostatic experiments performed on solid cylinders of amphibolite. The experiments described here are a subset of a larger group of experiments that were conducted to obtain mechanical data, which are described in another paper (Hacker and Christie, 1990). This study investigated disequilibrium transformations during deformation—no attempt was made to reach chemical equilibrium. The experiments shed light on the development of textures during prograde metamorphism of amphibolite, the effects of stress and deformation on metamorphism, and the compositions and textures of liquids formed during fusion of basaltic rock.

High-grade rocks visible on the Earth's surface do not preserve transient features that were present during metamorphism. For example, studies of anatexis, including the compositional and textural relationships among the liquid and restite phases, are hindered in rocks by the fact that the liquid may have moved away from its source region and that investigation can be conducted only after the liquid has crystallized. As a result, many details concerning reaction mechanisms and the development of metamorphic textures remain obscure. There are two basic approaches to laboratory experiments that can be conducted to overcome these inherent limitations. The first, a widely used approach, is to study powdered material with an emphasis on understanding compositions and modal proportions of phases at equilibrium. The disadvantage of this approach is that rocks are rather tightly packed polycrystalline aggregates, unlike powder, and consequently some information about reaction textures is lost. The second approach is to use solid pieces of rock to investigate reaction kinetics, compositions, and modal proportions of phases involved in the reactions. Although this approach provides information about reaction textures in a crystalline rock, it does have several disadvantages. Rates of reaction are slow because fluid must diffuse along grain boundaries (instead of between powder fragments), and the surfaces of grains are not free. This means that equilibrium may not be attained during the duration of the experiment and the fine-grained reaction

* Present address: Department of Geology, Stanford University, Stanford, California 94305-2115, U.S.A.

0003–004X/90/1112–1349$02.00

products must often be analyzed by time-consuming, high-resolution techniques such as transmission electron microscopy (Brearley, 1987; Rubie and Brearley, 1987). Moreover, because of time limitations, the slow heating that occurs during most natural environments cannot be duplicated in the laboratory. In spite of these disadvantages, experiments on solid pieces of rock do provide otherwise unavailable information about reactions that is complementary to the equilibrium approach using rock powders.

The solid pieces of rock used in this study provide the first opportunity to characterize the textural and chemical relationships among the phases involved in the transition from amphibolite to granulite facies in experimentally deformed basaltic rocks. These are the first experiments of this type at high pressure using unpowdered rock and the first using unpowdered mafic rock.

Melting studies of basaltic materials have been restricted to equilibrium studies conducted with rock powders (Yoder and Tilley, 1962; Green and Ringwood, 1968; Hill and Boettcher, 1970; Holloway and Burnham, 1972; Green, 1972; Eggler, 1972; Cawthorn et al., 1973; Helz, 1975; Spulber and Rutherford, 1983; Ellis and Thompson, 1986; Baker and Eggler, 1987; Beard and Lofgren, 1989, 1990). During this study, small melt fractions at quite low temperatures were produced, leading to an interesting comparison with previous studies and providing information about the composition and distribution of initial disequilibrium liquids in fused mafic rock.

A fundamental assumption in petrology is that the mechanisms, rates, and equilibrium conditions of transformations are not affected by deformation or deviatoric stress. Equilibrium conditions are normally modeled using hydrostatic thermodynamics, in which only the mean stress is considered to affect the internal energy of a phase; any effect that might be produced by strain or deviatoric stress is neglected in the hope that the effect is small. Theoretical expansions of Gibbs's (1906) treatment of thermodynamics by Kamb (1961), Fletcher (1973), Paterson (1973), Robin (1974), Green (1980, 1986), Heidug and Lehner (1985), Bayly (1985), and Kirby (1987) have shown, however, that the deviatoric components of a nonhydrostatic stress field affect, and in some cases even dominate, the thermodynamic potential of phases. The extent to which mechanical processes affect chemical processes is essentially unknown because of lack of investigation but could be considerable. In the present study, some samples were hydrostatically heated and some samples were deformed. By comparing the two sets of samples, we can evaluate the changes in phase compositions produced by stress and deformation.

Experimental procedure

The experiments were conducted in a piston-cylinder apparatus for studies of rock deformation (using solid pressure media) of the type designed by Griggs and coworkers (Griggs, 1967; Blacic, 1971). This paper discusses only experiments conducted on natural rock, although

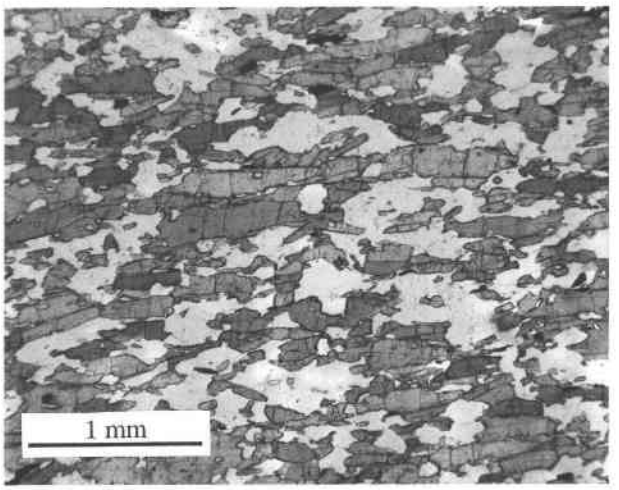

Fig. 1. Optical micrograph of the natural amphibolite starting material. Dark crystals are amphibole and minor ilmenite, and pale crystals are plagioclase and minor quartz.

many similar experiments were also performed on synthetic rock (Hacker and Christie, 1990). The starting material is an amphibolite composed of roughly 53% amphibole, 43% plagioclase, 2% ilmenite, 2% quartz, and trace amounts of rutile, sphene, and apatite (Fig. 1). The peak metamorphic temperature of this rock can be estimated as 600 ± 50 °C, using Spear's (1980) NaSi = CaAl exchange thermometer for amphibole and plagioclase. The rock has a uniform granoblastic texture and unzoned minerals, both of which help identify experimentally produced textural and chemical changes. The amphibole is tschermakitic hornblende (classification of Leake, 1978; Table 1). No other hydrous phases were detected with the electron microprobe or scanning transmission electron microscope; hence an experiment begun under vapor-absent conditions can only become hydrous when the amphibole dehydrates. The plagioclase is An_{30} (Table 2).

Samples of the natural rock were right circular cylinders, 6.25 mm in diameter and 12.7 mm in length, cored with a H_2O-cooled diamond drill. The samples were all tested in assemblies designed for deformation experiments so that differences in assembly design do not hinder comparison of deformed and hydrostatically heated samples. In H_2O-absent experiments, the sample was placed inside a Cu cylinder 2 mm thick below a cylinder of boron nitride (Fig. 2A). In experiments to which 1 wt% H_2O was added, the sample was placed inside a cylindrical Ag jacket 0.1 mm thick surrounded by talc (Fig. 2B). Ag is permeable to H_2 (Chou, 1987), and H_2 produced during amphibole and talc dehydration presumably diffused through the Ag jacket during the experiments, and thereby affected volatile fugacities. H_2O was transferred by pipette onto the top of the sample after the sample had been inserted into the Ag jacket. The H_2O was then mechanically sealed within the jacket by two ceramic end pieces (Fig. 2B). Each experiment was taken to the desired pressure and temperature in such a way that the

TABLE 1. Compositions of amphibole crystals

Experiment no.	TM8	1157	1159	1176	1177	1186	1189	1190	1191	1192	1194	1195	1197	1206	1207	1208	1279
Analysis	—	57	57	11	13	16	43	77	23	20	47	26	34	64	45	41	19
Reaction	—	3	3	2	2	3	2	1	1	3	3	1	1	1	3	3	4
Compositions in wt%																	
SiO_2	43.4 → 43.8	45.11	44.91	44.55	45.76	44.68	44.55	44.92	50.86	44.36	44.53	45.48	50.28	44.30	45.48	47.35	41.90
Al_2O_3	13.5 → 13.9	14.03	13.54	14.83	13.74	14.31	13.96	13.66	8.94	14.43	10.90	13.96	12.53	12.98	10.37	8.67	12.96
TiO_2	0.96 → 1.00	0.79	0.69	0.54	0.67	0.46	0.64	0.72	0.56	0.80	0.87	0.44	0.92	0.74	1.50	0.95	3.32
FeO*	14.4 → 14.6	13.64	13.66	17.78	13.83	12.94	13.78	13.66	13.78	14.12	17.39	13.07	11.87	14.13	15.75	15.35	15.11
Cr_2O_3	b.d. → 0.04	b.d.	b.d.	b.d.	0.05	0.09	0.04	b.d.	b.d.	0.07	0.06	b.d.	b.d.	b.d.	b.d.	0.03	0.07
MnO	0.27 → 0.30	0.18	0.27	0.39	0.24	0.25	0.27	0.32	0.13	0.30	0.23	0.25	0.25	0.31	0.23	0.29	0.17
MgO	11.5 → 11.6	10.54	12.04	7.97	11.12	11.08	11.60	11.46	13.13	10.94	10.96	11.81	8.79	12.26	12.14	13.14	11.11
CaO	10.3 → 10.4	10.23	10.48	7.23	9.98	10.69	10.56	10.48	7.91	9.94	9.62	10.80	8.37	10.50	9.89	9.60	9.97
Na_2O	1.9 → 2.0	2.57	1.92	2.98	3.35	2.00	1.89	2.19	2.98	2.11	2.30	2.19	2.44	2.16	2.20	1.65	2.76
K_2O	0.28 → 0.30	0.17	0.22	0.24	0.24	0.21	0.26	0.22	0.24	0.20	b.d.	0.22	0.17	0.11	0.04	b.d.	0.18
Sum	97.15 → 97.48	97.26	97.73	96.51	98.98	96.71	97.55	97.63	98.53	97.27	96.86	98.22	95.62	97.49	97.60	97.03	97.55
Cations per 23 O atoms*																	
Si	6.26 → 6.32	6.55	6.42	6.47	6.55	6.49	6.40	6.46	7.11	6.38	6.49	6.50	7.34	6.36	6.55	6.77	6.12
$^{[4]}Al$	1.68 → 1.74	1.45	1.58	1.53	1.45	1.51	1.61	1.54	0.89	1.62	1.51	1.50	0.66	1.64	1.45	1.24	1.88
$^{[6]}Al$	0.60 → 0.62	0.95	0.70	1.01	0.87	0.94	0.76	0.78	0.58	0.82	0.37	0.85	1.50	0.56	0.31	0.23	0.35
Ti	0.10 → 0.11	0.09	0.07	0.06	0.07	0.05	0.07	0.08	0.06	0.09	0.10	0.05	0.10	0.08	0.16	0.10	0.36
Fe^{3+}	1.0 → 1.1	0.39	0.96	1.27	0.40	0.53	0.88	0.72	0.97	0.92	1.29	0.61	0.00	1.06	1.15	1.40	0.86
Cr	b.d. → 0.01	b.d.	b.d.	b.d.	0.01	0.01	0.00	b.d.	b.d.	0.01	0.01	b.d.	b.d.	b.d.	b.d.	0.00	0.00
Fe^{2+}	0.65 → 0.72	1.27	0.67	0.89	1.25	1.04	0.77	0.92	0.64	0.78	0.83	0.95	1.45	0.63	0.75	0.43	0.98
Mn	0.03 → 0.04	0.02	0.03	0.05	0.03	0.03	0.03	0.04	0.02	0.04	0.03	0.03	0.03	0.04	0.03	0.04	0.02
Mg	2.47 → 2.49	2.28	2.56	1.73	2.37	2.40	2.48	2.46	2.73	2.35	2.38	2.52	1.91	2.62	2.61	2.80	2.42
Ca	1.60 → 1.61	1.59	1.60	1.13	1.53	1.66	1.63	1.62	1.18	1.53	1.50	1.65	1.31	1.62	1.53	1.46	1.56
^{M4}Na	0.39 → 0.40	0.41	0.40	0.84	0.47	0.34	0.38	0.39	0.81	0.47	0.50	0.35	0.69	0.38	0.47	0.46	0.44
^{A}Na	0.14 → 0.16	0.31	0.14	0.00	0.46	0.23	0.15	0.23	0.00	0.12	0.16	0.26	0.00	0.22	0.14	0.00	0.34
K	0.05 → 0.06	0.03	0.04	0.05	0.04	0.04	0.05	0.04	0.04	0.04	b.d.	0.04	0.03	0.02	0.01	b.d.	0.03

Note: TM8 indicates starting material, reaction indicates the reaction that produced the amphibole crystal, and b.d. indicates below detection.
* Calculated according to Laird and Albee (1981).

TABLE 2. Compositions of plagioclase crystal rims

Experiment no.	TM8	1157	1159	1177	1186	1189	1190	1192	1194	1195	1197	1206	1207	1208	1279
Analysis	—	61	70	14	43	19	40	24/145	19	16	36	70	19	39	82
An	30	40	33	31	37	27	42	40	37	40	35	38	49	37	49
	±0	±3	±11	±6	±4	±1	±5	±3	±1	±1	±3	±1	±2	±3	±2
Reaction	—	3	3	2	3	2	1	3	3	1	1	3	3	3	4
Compositions in wt%															
SiO_2	60.19 → 60.56	57.24	62.42	61.45	58.18	61.69	57.38	58.16	57.72	58.02	59.35	58.52	55.96	58.86	55.01
Al_2O_3	24.6 → 24.8	25.56	25.92	25.17	25.14	24.50	25.88	25.91	25.85	26.47	25.76	26.06	27.68	25.32	27.65
TiO_2	0.02 → 0.03	0.04	0.03	b.d.	0.04	0.03	0.12	0.03	b.d.	b.d.	b.d.	b.d.	0.03	b.d.	0.05
FeO*	0.05 → 0.10	0.88	0.12	0.42	0.61	0.14	0.64	0.52	0.20	0.18	0.54	0.38	0.47	0.30	0.39
Cr_2O_3	b.d. → b.d.	b.d.	b.d.	0.06	b.d.	0.06	b.d.	0.05	0.03	0.06	b.d.	b.d.	b.d.	b.d.	0.05
MnO	b.d. → b.d.	b.d.	b.d.	0.05	0.08	0.03	0.03	b.d.	0.04	b.d.	b.d.	0.04	b.d.	b.d.	0.03
MgO	b.d. → b.d.	0.29	b.d.	b.d.	0.32	b.d.	0.44	b.d.	b.d.	b.d.	b.d.	b.d.	b.d.	b.d.	b.d.
CaO	6.30 → 6.66	8.49	5.66	5.90	7.67	5.51	8.97	8.36	7.42	8.19	7.49	7.86	10.26	8.18	10.50
Na_2O	8.09 → 8.26	6.56	6.72	7.42	6.62	8.34	5.98	6.59	7.14	6.81	7.90	7.05	5.77	6.84	5.42
K_2O	0.06 → 0.05	0.05	b.d.	0.11	b.d.	0.10	b.d.	b.d.	b.d.	0.06	b.d.	b.d.	0.05	b.d.	0.13
Sum	100.00	99.11	100.89	100.58	98.66	100.40	99.48	99.66	98.42	99.83	101.08	99.95	100.25	99.54	99.24
Cations per eight O atoms*															
Si	2.70 → 2.70	2.60	2.72	2.71	2.64	2.73	2.59	2.61	2.62	2.60	2.63	2.62	2.52	2.64	2.50
Al	1.30 → 1.30	1.37	1.33	1.31	1.34	1.28	1.38	1.37	1.38	1.40	1.35	1.37	1.47	1.34	1.48
Ti	0.00 → 0.00	0.00	0.00	b.d.	0.00	0.00	0.00	0.00	b.d.	b.d.	b.d.	b.d.	0.00	b.d.	0.00
Fe	0.00 → 0.00	0.03	0.00	0.02	0.00	0.01	0.02	0.02	0.01	0.00	0.00	0.01	0.02	0.01	0.00
Cr	b.d. → b.d.	b.d.	b.d.	0.00	b.d.	0.00	b.d.	0.00	0.00	0.01	b.d.	b.d.	b.d.	b.d.	0.01
Mn	b.d. → b.d.	b.d.	b.d.	0.00	0.00	0.00	0.00	b.d.	0.00	b.d.	b.d.	0.00	b.d.	b.d.	0.00
Mg	b.d. → b.d.	0.02	b.d.	b.d.	0.02	b.d.	0.03	b.d.	b.d.	b.d.	b.d.	b.d.	b.d.	b.d.	b.d.
Ca	0.30 → 0.30	0.41	0.26	0.28	0.37	0.26	0.43	0.40	0.36	0.39	0.36	0.38	0.49	0.39	0.51
Na	0.70 → 0.70	0.58	0.57	0.63	0.58	0.72	0.53	0.57	0.63	0.59	0.68	0.61	0.50	0.60	0.48
K	0.00 → 0.00	0.00	b.d.	0.01	b.d.	0.01	b.d.	b.d.	b.d.	0.00	b.d.	b.d.	0.00	b.d.	0.01

Note: An refers to the mole fraction anorthite calculated as the average and maximum deviation from the average of 1 − Na, Ca, 3 − Si, and Al − 1. TM8 indicates starting material; compositions shown are for crystals that are the most different from each other. Reaction indicates the reaction that produced the plagioclase crystal, and b.d. indicates below detection.
* Calculated according to Laird and Albee (1981).

specific volume of H_2O remained less than one. The mechanical seal retains some H_2O, because quartzite samples tested with identical assemblies are visibly wet at the end of experiments. The method by which the amphibolite samples were recovered at the end of the experiments (see below) did not permit us to make this observation on amphibolite.

A few samples were heated hydrostatically, but most were compressed axially at strain rates of 10^{-4}–10^{-7} s^{-1}. The differential stresses (as high as 2200 MPa) and confining pressures yielded mean stresses (pressures) of 0.7–2.1 GPa [mean stress = (differential stress + confining pressure × 3)/3]. The confining pressure measured was not corrected for friction within the assembly or the strength of the confining medium; the actual confining pressure on the sample is different from that measured by perhaps 10% (Edmond and Paterson, 1971).

The temperature was obtained by resistive heating of a stepped cylindrical graphite furnace surrounding the sample and confining medium; it was measured by two $Pt/Pt_{90}Rh_{10}$ thermocouples estimated to be accurate to ±5 °C for temperatures of 700–1000 °C. Temperature control was better than ±3 °C precision for most experiments. Temperatures were not corrected for pressure or differential stress effects on the thermocouple emf, which should result in an uncertainty of ±4–6 °C for temperatures of 700–1000 °C at a confining pressure of 1.0 GPa (Getting and Kennedy, 1970; Mao and Bell, 1971). Thermal gradients within the assemblies were minimized by using (1) ceramic end pieces, (2) stepped furnaces that generate more heat toward the ends, (3) metal jackets, and (4) placement of thermocouples in mechanically stable regions (George and Christie, 1979). The thermal profiles in the assemblies used in this study should be similar to those presented by Koch et al. (1989), or ~4–8 °C mm^{-1}. The temperatures reported here are for the center of the sample. The experiments were quenched rapidly at rates of ~30–45 °C s^{-1}. This rapid quench rate is made possible by the small thermal mass of the sample assembly and the rapid flux of room temperature H_2O circulating above, below, and through the pressure vessel. Quench crystals were found during examination of the products, but are all <0.1 μm in length.

One wt% H_2O was added to some samples. The fugacities of volatiles were not buffered because measurements of rock strength are affected by a buffer capsule. The f_{O_2} of the assembly and rock was measured in two hydrostatic experiments by including small amounts of elemental and oxide metals in hydrostatic experiments. In one experiment at 1000 °C without added H_2O, wüstite was oxidized and Ni remained reduced. In another experiment at 925 °C with 1 wt% added H_2O, Ni was oxidized and Cu remained reduced. These limits are broad, but establish that the f_{O_2} was not extremely reducing or oxidizing. The spatial distribution of reaction products was rather uniform within all samples, suggesting that enough time was available for the fluid to penetrate the whole sample.

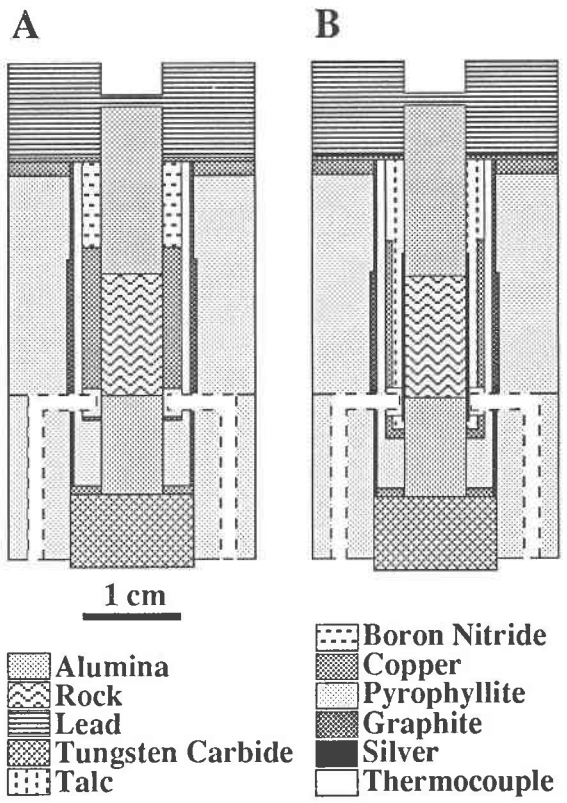

Fig. 2. Assemblies used in experiments (**A**) without and (**B**) with added H_2O.

After each experiment the sample jacket was removed incrementally with a lathe. Chemical treatment to remove the jacket or confining medium was specifically avoided to preserve the composition of the sample. The sample was then impregnated with resin and sawed in half lengthwise. The compositions and textures of the experimental products were systematically analyzed by an optical microscope, the electron microprobe including analysis with backscattered electrons, and the scanning transmission electron microscope to elucidate the physical and chemical processes that occurred during the experiments. Chemical reactions were identified by the appearance of new phases or the recrystallization or disappearance of preexisting phases. Samples tested for long durations (hundreds of hours) developed textural and chemical changes identifiable by backscattered electron microscopy and electron probe microanalysis. Scanning transmission electron microscopy was necessary to identify chemical or textural changes in samples tested for shorter durations. Liquid volumes were determined from backscattered electron micrographs; reported volumes as small as 1% are subject to ~100% uncertainty.

Micrometer-scale textural observations and chemical analyses of the phases were all made at UCLA with a four-spectrometer Cameca Camebax electron-probe microanalyzer and a single set of well-characterized natural and synthetic mineral standards; this is important be-

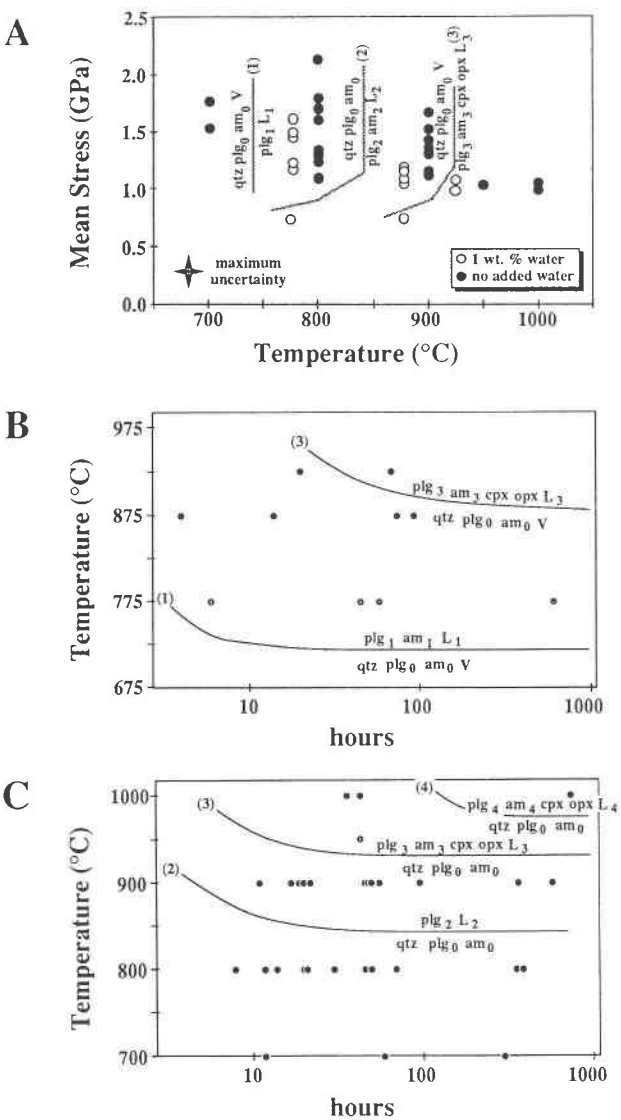

Fig. 3. (**A**) Temperatures and mean stresses (pressures) of the experiments. The reactions labeled 1 through 4 are discussed in the text. Abbreviations are qtz = quartz; plg = plagioclase; am = amphibole; V = vapor; L = liquid; opx = orthopyroxene; cpx = clinopyroxene. Different compositions of the same phase on opposite sides of a reaction are indicated by different subscripts. (**B**) Time-temperature-transformation relations for samples tested with 1 wt% added H_2O at 1.0 GPa confining pressure. Because experiments were not conducted at temperatures <775 °C, there is no lower temperature bracket for the position of Reaction 1. Note that the position of Reaction 3 is constrained by only 1 point. (**C**) Time-temperature-transformation relations for samples tested without added H_2O at 1.0 GPa confining pressure. Note that the position of Reaction 4 is constrained by only 1 point.

cause many of the changes in phase composition are small. Spot selection and textural analysis were performed in the backscattered electron mode to ensure that only single phases were analyzed and to facilitate the identification of phase zoning. The electron beam diameter was 2 μm, at 15 kV and 10 nA. For the analysis of glasses a beam diameter of 20 μm was used. Count times for each analysis were 20 s for peak intensities and 10 s for background intensities. Detection limits at these conditions are a function of phase composition, but for crystalline phases in this study, conservative limits are approximately 0.02 wt% for SiO_2, Al_2O_3, TiO_2, Cr_2O_3, and MnO, 0.03 wt% for FeO_{tot}, MgO, and CaO, 0.04 wt% for K_2O, and 0.05 wt% for Na_2O. The apparent large volatile contents of the glasses (~10 wt%) may be a result of using mineral standards, or it could be that the quenched liquids actually contain ~10% volatiles—the solubility of H_2O-rich fluid in tholeiitic glass quenched from pressures of ~1.0 GPa is ~10 wt% (Merzbacher and Eggler, 1984). Experimentation with the use of reduced counting and broad-beam techniques to measure glass compositions revealed that a beam diameter of 20 μm provided minimum alkali volatilization and correct metal concentrations.

A JEOL JEM 100-CX Temscan microscope, equipped with a beryllium double-tilt goniometer stage, was used in the transmission mode to characterize the submicroscopic structure and in the scanning and transmission modes with a Kevex®-Ray 3203-100c-VS energy-dispersive X-ray detector connected to a Tracor™ Northern NS-880 analysis system for phase identification.

Results

The conditions of the experiments (Fig. 3A; Table 3) correspond to the amphibolite, granulite, and eclogite metamorphic facies. Experiments were conducted for periods of up to 795 h at temperatures of 700–1000 °C and confining pressures of 0.5–1.5 GPa. The duration of each deformation experiment was chosen to satisfy certain rheological criteria (Hacker and Christie, 1990) and has no specific relation to metamorphic changes discussed in this paper. For example, no attempt was made to reach chemical equilibrium or evaluate the stability of phases by varying experiment duration. Conversely, the durations of the hydrostatic experiments were chosen to evaluate the effect of stress and deformation or to evaluate the stability of phases.

Textures of reactions

At the lowest temperature, 700 °C, the starting material was unchanged chemically and mineralogically—even in experiments of 297 h. Because the experiments were not reversed, this lack of change probably reflects slow reaction kinetics; recrystallization may well occur at these conditions during geologic time. At higher temperatures a sequence of reactions occurred (Fig. 3). In the presence of 1 wt% H_2O, melting occurred at 775 °C by the reaction

$$1.6\ \text{quartz} + 1.9\ \text{plagioclase}_0 + 0.84\ \text{amphibole}_0 + 3.5\ H_2O \rightarrow 1.2\ \text{plagioclase}_1 + 0.88\ \text{amphibole}_1 + 10\ L_1. \quad (1)$$

(The subscripts 0 and 1 are used to indicate that the reactant and product crystals are different in composition.) The stoichiometric coefficients were determined by least-

TABLE 3. Experimental conditions

T (°C)	Time (h)	P_c (GPa)	P (GPa)	H_2O	Stress (MPa)	log(é) (s^{-1})	Experiment no.
700	12	1.02	1.02	0	?	−4	1166
700	59	1.08	1.78	0	2099	−6	1139
700	297	1.10	1.06	0	1180	−7	1217
700–750	81	1.02	1.57–1.76	0	1661–2231+	−5,−6	1138
775	6	1.04	1.35–1.47	1	919–1279	−5,−4	1193
775	45	1.05	1.28	1	700	−6	1191
775	58	0.50	0.74	1	708	−6	1205
775	611	1.04	1.10	1	189	−7	1195
800	8	1.02	1.61	0	1781	−5	1162
800	12	1.09	1.09	0	?	−4	1163
800	14	1.44	1.44	0	?	−4	1185
800	20	1.11	1.59	0	1450	−5	1173
800	20	1.05	1.48–1.57	0	1279–1550	−5,−4	1203
800	21	1.06	1.01	0	1475	−4	1216
800	30	1.06	1.18–1.49	0	360–1300	−6,−5,−4	1136
800	46	1.05	1.23	0	545	−6	1146
800	50	1.54	2.14	0	1785	−6	1187
800	70	1.05	1.50	0	1356	−6	1175
800	351	1.52	1.78	0	790	−7	1202
800	388	1.04	1.28	0	721	−7	1160
800–900	69	1.08	1.30–1.71	0	665–1900	−6,−5,−4	1178
875	4	1.12	1.20–1.27	1	236–441	−5,−4	1190
875	14	1.04	1.04	1	?	−5	1196
875	74	1.09	1.16	1	222	−6	1197
875	93	0.50	0.75	1	747	−6	1206
900	11	1.08	1.42	0	1009	−4	1164
900	17	1.02	1.34	0	965	−5	1161
900	19	1.03	1.18–1.32	0	441–889	−6,−5,−4	1189
900	20	1.06	1.38–1.48	0	965–1254	−5,−4	1204
900	22	1.53	1.53	0	?	−5	1176
900	46	1.50	1.67	0	501	−6	1188
900	48	1.00	1.08–1.27	0	231–822	−6,−5,−4	1137
900	56	1.01	1.15	0	430	−6	1148
900	96	1.52	1.52	0	?	−6	1177
900	361	1.02	1.11	0	280+	−7	1174
900	579	1.51	1.68	0	501	−7	1201
900–950	50	1.10	1.31–1.42	0	351–970	−6,−5	1186
925	20	1.06	1.08	1	n/a	−5	1194
925	69	1.01	1.01	1	374	−6	1192
925	69	1.00	1.00	1	n/a	Hydro	1207
950	36	1.01	1.05	0	115	−6	1159
1000	43	1.00	1.00	0	n/a	Hydro	1208
1000	43	1.02	1.06	0	115	−6	1157
1000	795	1.00	1.00	0	n/a	Hydro	1279

Note: P_c = average confining pressure; P = minimum and maximum mean stress during mechanical steady state deformation; H_2O = wt% H_2O added; Stress = minimum and maximum differential stress (σ_1–σ_3) during mechanical steady state deformation (MPa); n/a = samples were not deformed during hydrostatic experiments; ? = stress measurement inaccurate because of high friction, motor failure, or excessive temperature fluctuation; log(é) = base-10 logarithm of the strain rates.

squares regression, using the modal proportions of reaction products, rim compositions of reactant and product phases, and liquid molar volumes from Lange and Carmichael (1987). They are highly uncertain because the product phases are typically zoned, the modal proportions of product phases are different in different reaction domains, and the volatile contents of the glasses are not well determined. Reaction 1 produced pools of liquid at amphibole-plagioclase-quartz triple junctions, resorption of quartz crystal margins, and growth of topotactic, euhedral rims on plagioclase and amphibole crystals that are compositionally different from the crystal cores (Fig. 4A). Reaction 1 typically produced ≤1 vol% liquid in all samples, regardless of experiment duration. This suggests that the amount of liquid is controlled by the amount of added H_2O, but lack of experimental reversal does not preclude the possibility that this reaction texture is metastable.

The same kind of textural and chemical evidence indicates that a similar reaction occurred in samples tested without added H_2O at 900 °C (Fig. 4B):

$$1.3\ \text{quartz} + 0.7\ \text{plagioclase}_0 + 0.1\ \text{amphibole}_0 + 2.6\ H_2O \rightarrow 0.05\ \text{plagioclase}_2 + 0.05\ \text{amphibole}_2 + 10\ L_2. \quad (2)$$

This reaction also produced <1 vol% liquid in all samples. It is not possible to balance this reaction without H_2O, even though no H_2O was added to the samples. This implies that H_2O adsorbed to the sample participated in the reaction, or that the inferred H_2O content of the quenched liquid is too high, or both.

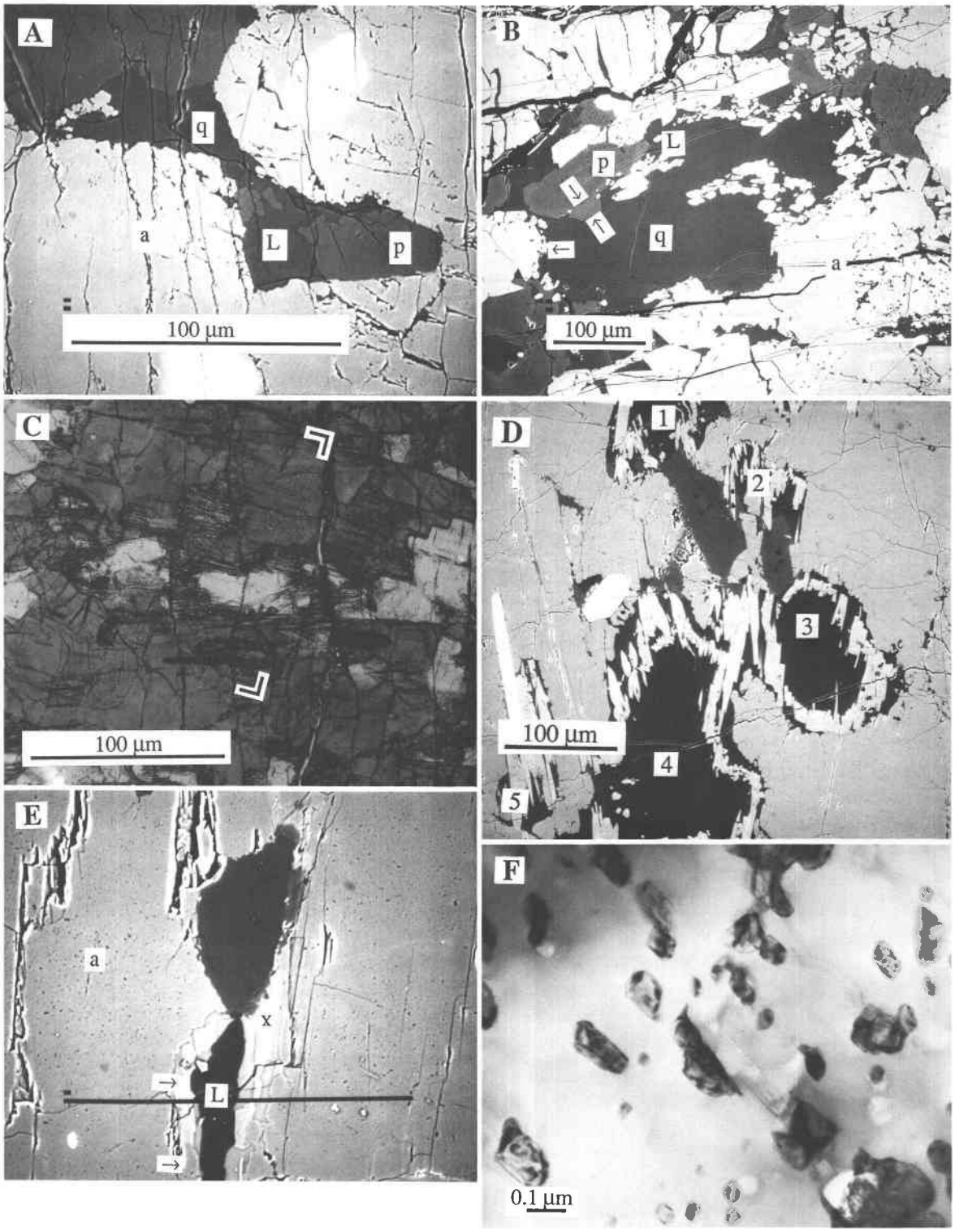

Fig. 4. Backscattered electron micrographs illustrating the amphibolite-to-granulite facies reaction textures. The obvious cracks in all photos occurred during unloading and cooling at the end of each experiment. (**A**) Reaction 1: hornblende (a), plagioclase (p), quartz (q), and H_2O react to produce liquid (L) and cause minor recrystallization of amphibole and plagioclase. (**B**) Reaction 2: dehydration melting of hornblende (a), plagioclase (p), and quartz (q) to produce liquid (L), leading to growth of magnesio-hornblende and calcium plagioclase rims (arrows). (**C**) General texture of Reaction 3 viewed with an optical microscope. (**D**) Same area as in (**C**) showing five numbered, separate domains of reaction. (**E**) Early stages of Reaction 3, illustrating the incipient growth of pyroxene crystals (x) into liquid (L) from their amphibole substrate (a); arrows indicate the transect illustrated in Figure 8. (**F**) Transmission electron micrograph of pyroxene neoblasts (dark) nucleated in amphibole (light).

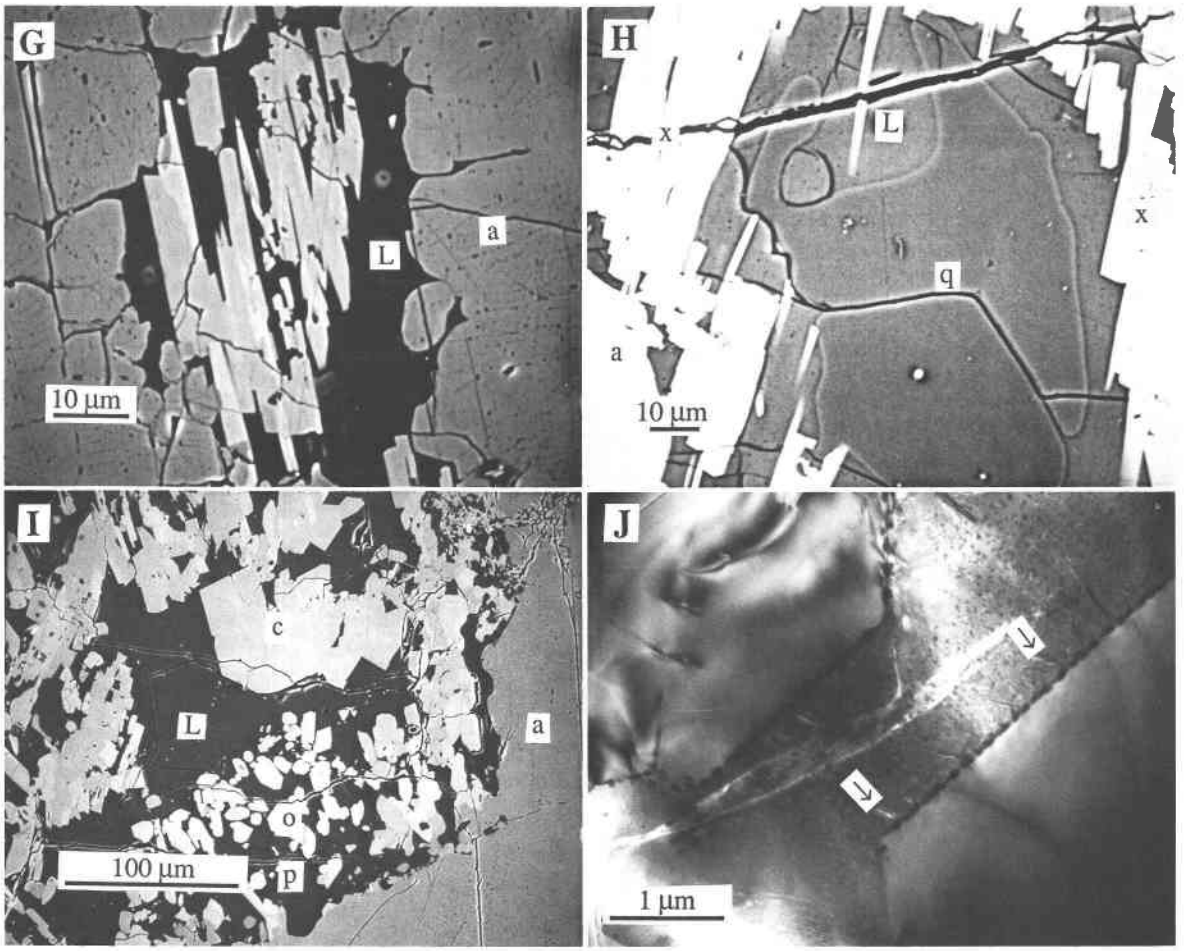

Fig. 4—*Continued.* (**G**) Intergrown hypersthene (brighter) and augite (darker) crystals grown in a liquid-filled cavity (L) in resorbed amphibole (a). (**H**) Detail of textural relationships among amphibole (a), quartz (q), pyroxene (x), and liquid (L). (**I**) Most evolved textures from Reaction 4 showing orthopyroxene (o), clinopyroxene (c) occupying a large area filled with liquid (L) and plagioclase (p) adjacent to amphibole (a). (**J**) Transmission electron micrograph of quench crystals (arrow) grown on pyroxene neoblasts.

At the highest temperatures (875–1000 °C; Figs. 3, 4C, and 4D), pyroxenes were produced by the reaction

$$3.2\ \text{quartz} + 0.3\ \text{plagioclase}_0 + 0.5\ \text{amphibole}_0 + 1.6\ H_2O \rightarrow 0.2\ \text{plagioclase}_3 + 0.1\ \text{amphibole}_3 + 0.7\ \text{augite}_3 + 0.5\ \text{hypersthene}_3 + 10\ L_3. \quad (3)$$

In the early stages of Reaction 3, pyroxene neoblasts appear along liquid-filled amphibole-quartz grain boundaries (Figs. 4E, 4F). Liquid compositions indicate that plagioclase was also a minor reactant. The pyroxenes nucleated on {*hk*0} amphibole faces, and the orientation of pyroxene *a, b,* and *c* axes was inherited from the host amphibole. The ortho- and clinopyroxene crystals grow side by side with parallel *c* axes (Fig. 4G). In their early stages of growth (typically less than 20 μm long), the pyroxene crystals remain in contact with their host amphibole, and the liquid film between the pyroxene and quartz crystals widens. The pyroxene crystals did not nucleate along amphibole-plagioclase contacts, and pyroxene and plagioclase are in contact without an apparent reaction relationship. Later, the pyroxene crystals grew away from the host amphibole into the liquid and avoided contact with all other crystals. Simultaneously, the host amphibole receded from the pyroxene nucleation site. The texture at this stage consists of embayed quartz and amphibole crystals separated by liquid containing a layer of intergrown ortho- and clinopyroxene crystals (Fig. 4H). Eventually, all the quartz is consumed (Fig. 4I) by the reaction

$$4.2\ \text{quartz} + 0.42\ \text{plagioclase}_3 + 1.3\ \text{amphibole}_3 + 0.6\ H_2O \rightarrow 1.2\ \text{plagioclase}_4 + 0.08\ \text{amphibole}_4 + 1.8\ \text{augite}_4 + 1.8\ \text{hypersthene}_4 + 10\ L_4. \quad (4)$$

Reactions 3 and 4 occur at ≥925 °C and 1.0 GPa and at ≥875 °C and 0.75 GPa.

The products of the above four reactions are easily dis-

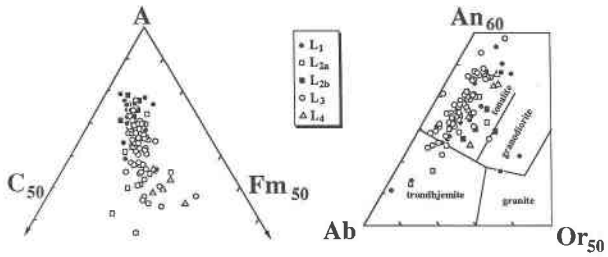

Fig. 5. Quenched liquid compositions. ACF molar ternary diagram: A = Al_2O_3-Na_2O-K_2O; C = CaO; F = FeO* + MgO, and CIPW-normalizations shown as molar fractions of feldspar end-members (after Barker, 1979). The compositions of all five liquids overlap.

tinguished from quench crystals, which are tiny acicular crystals (<0.1 μm) observed on the faces of coarser crystals (Fig. 4J).

Phase compositions

The quenched liquid in all samples is corundum normative and similar to tonalite (Fig. 5; Table 4). Compositional gradients within individual quenched liquid pools were not detected with analyses at 1-μm or 2-μm intervals using the electron probe, but each liquid pool typically is compositionally different from neighboring pools. This implies that (1) diffusion is rapid within each liquid pool, (2) there is incomplete diffusion between neighboring pools, and (3) each pool formed by a slightly different reaction. L_3 and L_4 liquids contain more TiO_2 and FeO_{tot}, generally more MgO, and less Na_2O and K_2O than L_1 and L_2 liquids (cf. Beard and Lofgren, 1989, 1990); i.e., the higher temperature liquids are relatively enriched in some amphibole components (Table 4). These differences are so small, however, that they are not apparent in Figure 5. At temperatures between Reactions 3 and 4, quenched liquid compositions do not depend on temperature. L_4 liquids contain less SiO_2 and more Al_2O_3 and K_2O than L_3 liquids (compare experiments 1208 and 1279 in Table 4).

The pyroxene crystals grown in all experiments are chiefly augite and hypersthene (Table 5). There are no marked differences in the compositions of pyroxenes grown in different samples (Fig. 6), further indication of the lack of equilibrium. Figure 7 illustrates the compositional change characterizing the amphibole-to-pyroxene transformation. The rim of the host amphibole crystal contains less MgO and FeO_{tot} and more Al_2O_3 and SiO_2 than the core of the host amphibole crystal. The greatest compositional change occurs across the amphibole-pyroxene interface.

The tschermakitic hornblende crystals in the starting material are variably altered to magnesio-hornblende principally through Mg-Tschermak substitution,

TABLE 4. Compositions of quenched liquid

Liquid	1	1	1	1	1	1	1	2	2	2	2	2
Experiment no.	1190	1191	1193	1195	1196	1197	1206	1177	1186	1161	1164	1176
Analysis	18	21	25	28	30	33	99	12	41	4	6	8
						Compositions in wt%						
SiO_2	74.88	78.32	77.17	75.23	75.38	76.99	77.39	74.03	72.72	76.94	77.60	76.27
Al_2O_3	15.75	14.45	15.57	16.65	17.78	15.64	14.35	15.71	14.96	14.98	15.70	16.38
TiO_2	0.12	0.06	0.04	0.07	0.11	0.05	0.28	0.07	0.18	0.07	0.17	0.10
FeO*	2.05	1.31	0.83	1.04	0.66	1.38	2.26	1.59	2.46	1.50	1.40	0.75
Cr_2O_3	b.d.	b.d.	b.d.	b.d.	0.07	b.d.	0.07	b.d.	b.d.	b.d.	b.d.	b.d.
MnO	b.d.	b.d.	0.06	b.d.	0.09	0.05	0.09	0.08	0.09	b.d.	b.d.	0.04
MgO	0.52	0.54	0.17	0.39	0.21	0.25	0.29	0.84	1.83	0.34	0.40	0.26
CaO	3.24	1.22	2.40	2.87	3.38	2.70	2.45	3.50	3.98	2.44	2.19	2.34
Na_2O	2.84	2.35	3.12	3.01	1.76	2.49	2.34	3.39	2.84	2.63	1.77	2.39
K_2O	0.56	1.74	0.63	0.73	0.55	0.45	0.49	0.77	0.95	1.04	0.78	1.45
Sum	88.66	87.38	87.49	86.63	82.31	87.39	88.93	86.36	88.66	88.98	83.06	81.29

Liquid	2	3	3	3	3	3	3	3	3	3	3	4	4
Experiment no.	1204	1157	1157	1159	1192	1192	1194	1207	1207	1208	1208	1279	1279
Analysis	38	63	69	53	16	19	46	34	37	54	60	78	79
						Compositions in wt%							
SiO_2	76.29	74.73	80.25	77.49	76.19	74.98	75.65	66.24	73.11	77.40	74.25	67.39	64.26
Al_2O_3	15.08	14.42	11.38	13.62	13.10	15.21	15.57	13.01	7.59	14.72	13.97	18.76	17.48
TiO_2	0.09	0.41	0.32	0.22	0.26	0.28	0.20	0.64	1.62	0.08	0.16	0.70	0.63
FeO*	1.01	3.14	2.24	2.11	3.10	2.11	1.09	7.51	6.71	1.71	2.53	3.41	6.14
Cr_2O_3	b.d.	b.d.	b.d.	b.d.	b.d.	0.05	b.d.	b.d.	0.04	b.d.	b.d.	0.04	b.d.
MnO	0.10	b.d.	0.04	0.08	0.09	0.03	b.d.	0.15	0.17	0.04	0.05	0.05	0.08
MgO	0.18	0.47	0.37	1.15	0.60	0.42	0.08	4.37	3.59	0.37	1.64	0.48	2.07
CaO	2.64	3.05	2.33	2.46	2.63	2.79	2.59	4.88	4.99	3.02	4.82	4.95	5.37
Na_2O	3.51	3.12	2.54	2.18	3.65	3.68	4.30	2.75	1.87	2.21	2.18	2.93	2.71
K_2O	1.09	0.64	0.52	0.70	0.38	0.45	0.53	0.43	0.31	0.44	0.40	1.30	1.26
Sum	88.81	91.09	90.83	88.16	90.24	88.77	90.05	92.59	95.28	87.62	87.62	89.94	91.88

Note: Compositions are adjusted to 100% totals, with original total shown; b.d. = below detection.

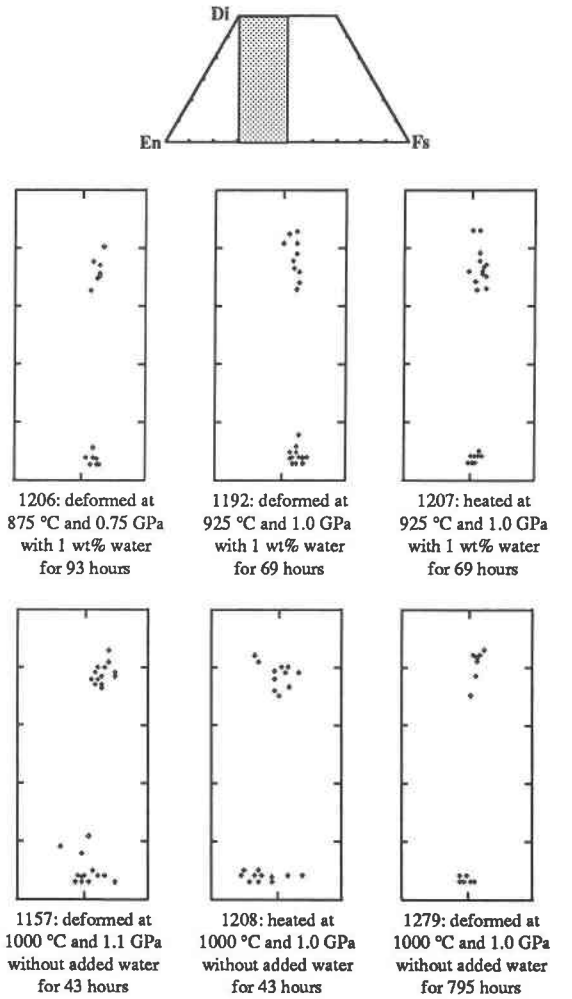

Fig. 6. Compositions of pyroxene crystals shown as solid solutions of Wo (Ca), En (Mg), and Fs (Fe^{2+}) end-members. Subcalcic augite and intermediate pigeonite are discrete phases on the scale of micrometers and not mixed analyses of adjacent augite and hypersthene. There are no systematic differences among the compositions of pyroxenes formed in different experiments.

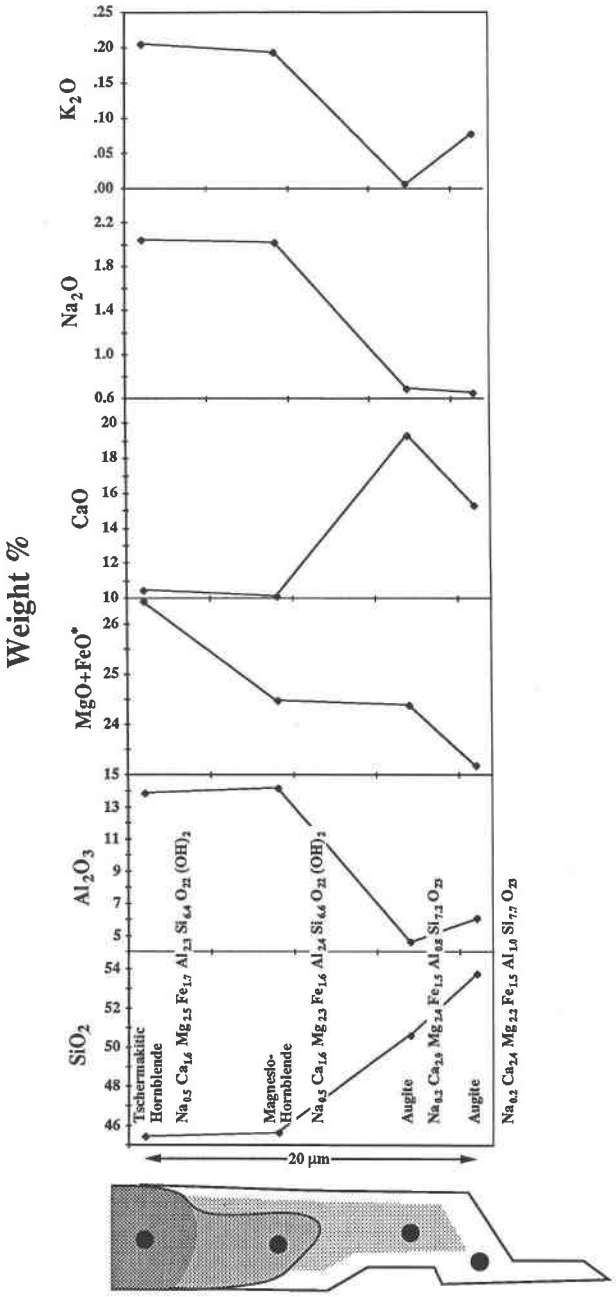

Fig. 7. Composition of an interface between a host amphibole crystal and a pyroxene neoblast. The amphibole and pyroxene formulae are normalized to 15 cations for comparison.

$MgSi^{[6]}Al_{-1}{}^{[4]}Al_{-1}$ (Figs. 4B and 8; Table 1). The magnitude of substitution varies from domain to domain, indicating a lack of sample-scale equilibrium.

Recrystallized plagioclase crystals are zoned, with sodic cores (An_{28-30}) and euhedral calcic rims (An_{31-56}; Fig. 4; Table 2). The anorthite content of the plagioclase crystals produced in Reaction 3 is less than that produced in Reaction 2, although generally the changes in plagioclase composition are not systematic functions of temperature, pressure, or experiment duration (cf. Beard and Lofgren, 1990).

Discussion

Textures

As mentioned previously, the peak metamorphic temperature of the starting material was roughly 600 ± 50 °C. This means that experiments at 700 °C and 1000 °C overstep the equilibration temperature of the rock by 100 °C and 400 °C, respectively. Moreover, the rate at which the experimental samples were heated is not typical of natural metamorphism, except perhaps that of xenoliths entrained in magma.

This study investigated phase transformations during deformation. No attempt was made to reach equilibrium. Quartz is a reactant in all the reactions in this study, yet

TABLE 5. Compositions of pyroxene crystals

Experiment no.	1157	1157	1192	1192	1206	1206	1207	1207	1208	1208	1279	1279
Analysis	31/58	32/59	28/135	27/142	50	49	64	65	82	83	21	18
Pyroxene	Hyp	Aug	Hyp	Aug	Hyp	Aug	Hyp	Aug	Hyp	Aug	Hyp	Aug
						Compositions in wt%						
SiO_2	50.69	50.44	51.67	51.08	52.16	51.53	51.19	51.66	51.62	51.85	50.46	50.05
Al_2O_3	3.04	3.72	2.96	3.58	1.16	1.85	2.72	3.18	3.43	4.68	4.15	4.68
TiO_2	0.22	0.50	0.26	0.58	0.15	0.12	0.28	0.46	0.24	0.38	0.26	0.78
FeO*	23.13	14.45	24.59	13.81	24.96	14.13	23.23	14.57	21.60	9.19	23.61	12.36
Cr_2O_3	b.d.	b.d.	0.04	0.06	b.d.	0.05	0.11	0.12	0.09	0.05	b.d.	0.06
MnO	0.41	0.41	0.40	0.23	0.53	0.39	0.42	0.37	0.32	0.27	0.50	0.28
MgO	19.90	12.98	18.23	12.38	18.94	12.34	19.64	14.10	20.67	13.35	19.53	12.05
CaO	1.75	16.53	1.77	17.71	1.57	19.08	2.13	15.18	2.30	18.98	1.41	18.97
Na_2O	b.d.	0.59	0.07	0.54	b.d.	0.50	b.d.	0.31	0.07	0.89	b.d.	0.62
K_2O	b.d.	b.d.	b.d.	b.d.	b.d.	b.d.	b.d.	b.d.	b.d.	b.d.	b.d.	b.d.
Sum	99.17	99.62	99.99	99.97	99.47	99.99	99.72	99.95	100.34	99.64	99.92	99.85
						Cations per six O atoms*						
Si	1.92	1.91	1.95	1.93	1.98	1.96	1.93	1.94	1.92	1.93	1.90	1.89
$^{(4)}Al$	0.08	0.09	0.05	0.07	0.02	0.04	0.07	0.06	0.08	0.07	0.10	0.11
$^{(6)}Al$	0.06	0.08	0.09	0.09	0.03	0.04	0.05	0.08	0.07	0.13	0.08	0.10
Ti	0.01	0.01	0.01	0.02	0.00	0.00	0.01	0.01	0.01	0.01	0.01	0.02
Fe^{2+}	0.73	0.45	0.78	0.43	0.79	0.45	0.73	0.46	0.67	0.29	0.74	0.39
Mn	0.01	0.01	0.01	0.01	0.02	0.01	0.01	0.01	0.01	0.01	0.02	0.01
Mg	1.13	0.73	1.02	0.70	1.07	0.70	1.10	0.79	1.15	0.74	1.10	0.68
Ca	0.07	0.67	0.07	0.72	0.06	0.78	0.09	0.61	0.09	0.75	0.06	0.77
Na	b.d.	0.04	0.01	0.04	b.d.	0.04	b.d.	0.02	0.01	0.06	0.00	0.05

Note: Each pair of analyses for a single sample represents adjacent clino- and orthopyroxene crystals. Aug = augite; Hyp = hypersthene; b.d. = below detection.

* Calculated according to Robinson (1980).

it forms only ~2 vol% of the rock. The quartz grains are widely separated, such that the reaction domain centered about each quartz crystal remains spatially and chemically separated from nearby domains. Different crystals of a single phase within one reaction domain have reasonably homogeneous rims, but crystals of similar phases in different reaction domains are compositionally different. Consequently the stoichiometric coefficients of the above reactions inferred from product phase compositions and molar proportions vary from one domain to another. This indicates that although local equilibrium may have been achieved, equilibrium certainly was not attained on the scale of the entire sample. Many factors could contribute to the establishment of equilibrium within domains, including different dissolution rates of reactants and different nucleation and growth rates of products.

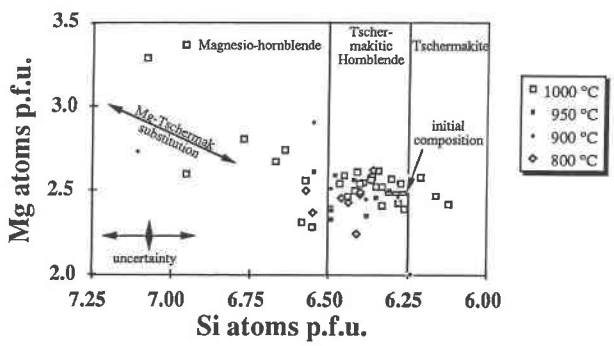

Fig. 8. Compositions of amphibole crystals. There is no correlation of temperature with composition, except that amphiboles from the lower temperature experiments are more like those in the starting material.

Two other studies have been conducted on unpowdered rocks with a view toward investigating transformation kinetics and mechanisms. Brearley (1987) heated a garnet-biotite-plagioclase-quartz gneiss without added H_2O at 800 °C and 100 MPa. As did pyroxene in this study, spinel and orthopyroxene grew in the gneiss and initially had orientations controlled by the host biotite crystals. As the liquid volume increased and the biotite was consumed, these topotactic relationships were lost. This change from initially coherent, minimum-energy interfaces with host crystals to incoherent interfaces with liquid occurs because the strain energy and surface energy of a phase are interdependent, and the fastest combined nucleation and growth occurs for those interfaces that minimize the sum of the two energies. Because surface energy is proportional to area and strain energy is proportional to volume, nuclei typically form with coherent interfaces (low surface energy and high strain energy) and then abandon them during growth for energetically more favorable incoherent interfaces (high surface energy and low strain energy) (Putnis and McConnell, 1980).

Effect of stress and deformation

This study provides limited indications of the effect of stress and deformation on metamorphism. The compositions of phases and the partitioning of elements among phases in undeformed and deformed samples are different. For example, hypersthene and liquid from deformed and undeformed samples are compositionally different. The greatest difference in compositions of liquid from

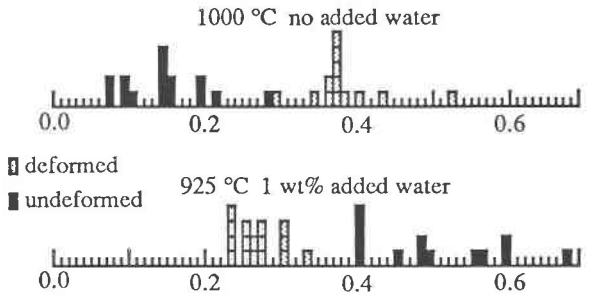

Fig. 9. Wt% TiO_2 contents of glasses from pairs of otherwise similar deformed and undeformed samples. For the experiments at 1000 °C (experiments 1157 and 1208), glass from the deformed sample is more titaniferous, whereas at 925 °C (experiments 1192 and 1207) glass from the undeformed sample is more titaniferous.

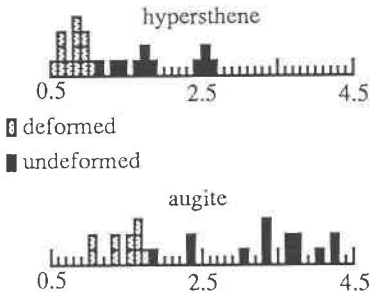

Fig. 10. TiO_2 partition coefficients between coexisting pyroxene and glass grown at 1000 °C (experiments 1157 and 1208). Both augite and hypersthene contain more TiO_2 relative to liquid in the deformed samples compared to the undeformed samples.

undeformed and deformed samples is in their TiO_2 content (Fig. 9). Hypersthene shows a similar relationship for FeO_{tot} and total oxide concentrations. Stress and deformation also affected element partitioning between pyroxenes and liquid (Fig. 10). Again, TiO_2 is the element affected to the greatest extent. These results indicate that stress and deformation can cause measurable changes in compositions of experimentally grown phases, although why the changes are most notable for TiO_2 is unknown. The partitioning occurred under conditions rather different from typical equilibrium partitioning experiments, and whether such behavior would occur under natural conditions cannot be evaluated. The effects of stress and deformation on phase compositions and element partitioning might be measured more effectively using a compositionally simpler system.

Relation to equilibrium studies

The results of this study can be compared with those of two phase-equilibrium studies on mafic compositions. In this study, melting of quartz + amphibole + plagioclase occurred in samples with 1 wt% added H_2O at 1.0 GPa and $\leq$775 °C. The 1986 study by Ellis and Thompson of the quartz-saturated CaO-MgO-Al_2O_3-SiO_2-H_2O (CMASH) system revealed the same reaction at ~775 °C. The non-CMASH components present in the natural material do not appear to depress the reaction temperature noticeably, but it should be noted that the melting reaction observed in this study may be metastable relative to some kinetically less favorable subsolidus reaction. In the study by Ellis and Thompson (1986), the high temperature products of this reaction were clinopyroxene + liquid, whereas calcic plagioclase + silicic amphibole + liquid were the reaction products in this study. Pyroxene was not produced in this study until temperatures of 925 °C were reached at 1.0 GPa.

Beard and Lofgren (1989, 1990) melted powdered greenschist- and amphibolite-facies basalt and andesite at 800–1000 °C and 100, 300, and 700 MPa under both H_2O-saturated conditions and without added H_2O. They found that dehydration melting of amphibole + plagioclase + quartz at 850 °C and 0.7 GPa produced about 5 vol% liquid. The same reaction in this study at 900 °C and 1.0 GPa produced <1 vol% liquid. Moreover, Beard and Lofgren (1989, 1990) documented that at 900 °C and 0.7 GPa, amphibole and quartz were entirely consumed to create clinopyroxene, orthopyroxene, plagioclase, and 20 vol% liquid. Amphibole was present in all samples in this study, and quartz was consumed only in one experiment, at 1000 °C for 795 h.

Thus, comparison with the equilibrium studies of Ellis and Thompson (1986) and Beard and Lofgren (1989, 1990) indicates that the reactions in this study did not progress to completion. The phase compositions and proportions produced are metastable and would presumably have been different if the experiments had been for longer durations. Previous studies of reactions using solid pieces of rock have also found evidence of disequilibrium. Metastable melting occurred in a quartz-muscovite schist heated by Rubie and Brearley (1987) with added H_2O at 680, 720, and 757 °C for 12 h to 5 months. Metastable corundum + mullite that formed early in the experiments was eventually replaced by the stable assemblage orthoclase + sillimanite + biotite + H_2O.

This study, along with those of Rubie and Brearley (1987) and Brearley (1987), demonstrates that solid pieces of rock can be used to investigate the textures and mechanisms that occur during the early stages of reactions, but later stages of reactions, particularly the equilibrium textures, cannot be investigated without experiments more than one month long because reaction rates are slow and metastable phases persist.

Acknowledgments

The manuscript was read and improved by L. Anovitz, J.S. Beard, A. Brearley, M. Cho, W.A. Dollase, T. Hoisch, and B.S. White. This work was funded by NSF Grant EAR84-16781 and a Sigma Xi research grant.

References cited

Baker, D.R., and Eggler, D.H. (1987) Compositions of anhydrous and hydrous melts coexisting with plagioclase, augite, and olivine or low-Ca pyroxene from 1 atm to 8 kbar: Application to the Aleutian volcanic center Atka. American Mineralogist, 72, 12–28.

Barker, F. (1979) Trondhjemite: Definition, environment, and hypotheses

of origin. In F. Barker, Ed., Trondhjemites, dacites, and related rocks, p. 1–12. Elsevier, Amsterdam.

Bayly, B. (1985) Deformation with simultaneous chemical change: The thermodynamic basis. In A.B. Thompson and D.C. Rubie, Eds., Metamorphic reactions: Kinetics, textures, and deformation, p. 269–277. Springer-Verlag, New York.

Beard, J.S., and Lofgren, G.E. (1989) Effect of water on the composition of partial melts of greenstone and amphibolite. Science, 244, 195–197.

——— (1990) Dehydration melting and water-saturated melting of greenstone and amphibolite at 1, 3, and 7 kb. Journal of Petrology, 31, in press.

Blacic, J.D. (1971) Hydrolitic weakening of quartz and olivine, 205 p. Ph.D. dissertation, University of California, Los Angeles, California.

Brearley, A.J. (1987) An experimental and kinetic study of the breakdown of aluminous biotite at 800 °C: Reaction microstructures and mineral chemistry. Bulletin de Minéralogie, 110, 513–532.

Cawthorn, R.G., Curran, E.B., and Arculus, R.J. (1973) A petrogenetic model for the origin of the calc-alkaline suite of Grenada, Lesser Antilles. Journal of Petrology, 14, 327–337.

Chou, I.-M. (1987) Oxygen buffer and hydrogen sensor techniques at elevated pressures and temperatures. In G.C. Ulmer and H.L. Barnes, Eds., Hydrothermal experimental techniques, p. 61–99. Wiley, New York.

Edmond, J.M., and Paterson, M.S. (1971) Strength of solid pressure media and implications for high pressure apparatus. Contributions to Mineralogy and Petrology, 30, 141–160.

Eggler, D.H. (1972) Water-saturated and under-saturated melting relations in a Paricutín andesite and an estimate of water content in natural magma. Contributions to Mineralogy and Petrology, 34, 261–271.

Ellis, D.J., and Thompson, A.B. (1986) Subsolidus and partial melting reactions in the quartz-excess CaO + MgO + Al_2O_3 + SiO_2 + H_2O system under water-excess and water-deficient conditions to 10 kb: Some implications for the origin of peraluminous melts from mafic rocks. Journal of Petrology, 27, 91–121.

Fletcher, R.C. (1973) Propagation of a coherent interface between two nonhydrostatically stressed crystals. Journal of Geophysical Research, 78, 7661–7666.

George, R.P., Jr., and Christie, J.M. (1979) Improved sample assemblies for the Griggs solid-medium deformation apparatus. Eos, 60, 371.

Getting, I.C., and Kennedy, G.C. (1970) The effect of pressure on the e.m.f. of chrome-alumel and platinum-platinum 10% rhodium thermocouples. Journal of Applied Physics, 41, 4552–4561.

Gibbs, J.W. (1906) On the equilibrium of heterogeneous substances. In H.A. Bumstead and R.G. Van Name, Eds., Collected works of J. Willard Gibbs. Yale University Press, New Haven, Connecticut.

Green, D.H., and Ringwood, A.E. (1968) Genesis of the calc-alkaline igneous rock suite. Contributions to Mineralogy and Petrology, 18, 105–162.

Green, H.W., II. (1980) On the thermodynamics of nonhydrostatically stressed solids. Philosophical Magazine, 41, 637–647.

——— (1986) Phase transformations under stress and volume transfer creep. In B.E. Hobbs and H.C. Heard, Eds., Mineral and rock deformation: Laboratory studies. AGU Monograph, 36, 201–211.

Green, T.H. (1972) Crystallization of calc-alkaline andesite under controlled high-pressure hydrous conditions. Contributions to Mineralogy and Petrology, 34, 150–166.

Griggs, D.T. (1967) Hydrolitic weakening of quartz and other silicates. Geophysical Journal of the Royal Astronomical Society, 14, 19–31.

Hacker, B.R., and Christie, J.M. (1990) Brittle/ductile and plastic/cataclastic transitions in experimentally deformed and metamorphosed amphibolite. The brittle-ductile transition in rocks, AGU Monograph 56, 127–147.

Heidug, W., and Lehner, F.K. (1985) Thermodynamics of coherent phase transformations in nonhydrostatically stressed solids. Pure and Applied Geophysics, 123, 91–98.

Helz, R.T. (1975) Phase relations of basalts in their melting ranges at PH_2O = 5 kb. Part II. Melt compositions. Journal of Petrology, 17, 139–193.

Hill, R.E.T., and Boettcher, A.L. (1970) Water in the earth's mantle: Melting curves of basalt-water and basalt-water-carbon dioxide. Science, 167, 980–982.

Holloway, J.R., and Burnham, C.W. (1972) Melting relations of basalt with equilibrium water pressure less than total pressure. Journal of Petrology, 13, 1–30.

Kamb, W.B. (1961) The thermodynamic theory of nonhydrostatically stressed solids. Journal of Geophysical Research, 66, 259–271.

Kirby, S.H. (1987) Localized polymorphic phase transformations in high-pressure faults and applications to the physical mechanism of deep earthquakes. Journal of Geophysical Research, 92, 13789–13800.

Koch, P.S., Christie, J.M., Ord, A., and George, R.P., Jr. (1989) Effect of water on the rheology of experimentally deformed quartzite. Journal of Geophysical Research, 94, 13975–13996.

Laird, J., and Albee, A.L. (1981) Pressure, temperature, and time indicators in mafic schist: Their application to reconstructing the polymetamorphic history of Vermont. American Journal of Science, 281, 127–175.

Lange, R.A., and Carmichael, I.S.E. (1987) Densities of Na_2O-K_2O-CaO-MgO-FeO-Fe_2O_3-Al_2O_3-TiO_2-SiO_2 liquids: New measurements and derived molar properties. Geochimica Cosmochimica Acta, 51, 2931–2946.

Leake, B.E. (1978) Nomenclature of amphiboles. Canadian Mineralogist, 16, 501–520.

Mao, H.K., and Bell, P.M. (1971) Behavior of thermocouples in the single-stage piston-cylinder apparatus. Carnegie Institution of Washington Year Book, 69, 207–216.

Merzbacher, C., and Eggler, D.H. (1984) A magmatic geohygrometer: Application to Mount St. Helens and other dacitic magmas. Geology, 12, 587–590.

Paterson, M.S. (1973) Nonhydrostatic thermodynamics and its geologic applications. Reviews of Geophysics and Space Physics, 11, 355–389.

Putnis, A., and McConnell, J.D.C. (1980) Principles of mineral behaviour, 257 p. Elsevier, New York.

Robin, P.-Y. (1974) Thermodynamic equilibrium across a coherent interface in a stressed crystal. American Mineralogist, 59, 1286–1298.

Robinson, P. (1980) The composition space of terrestrial pyroxenes—Internal and external limits. Mineralogical Society of America Reviews in Mineralogy, 7, 419–494.

Rubie, D.C., and Brearley, A.J. (1987) Metastable melting during the breakdown of muscovite + quartz at 1 kbar. Bulletin de Minéralogie, 110, 533–549.

Spear, F.D. (1980) NaSi = CaAl exchange equilibrium between plagioclase and amphibole. Contributions to Mineralogy and Petrology, 72, 33–41.

Spulber, S.D., and Rutherford, M.J. (1983) The origin of rhyolite and plagiogranite in oceanic crust: An experimental study. Journal of Petrology, 24, 1–25.

Yoder, H.S., Jr., and Tilley, C.E. (1962) Origin of basalt magmas: An experimental study of natural and synthetic rock systems. Journal of Petrology, 3, 342–532.

Manuscript received December 30, 1988
Manuscript accepted September 18, 1990